

## COMPRESSION BEHAVIORS OF CEMENTITIOUS CELLULAR COMPOSITES WITH NEGATIVE POISSON'S RATIO

YADING XU<sup>\*</sup>, BRANKO ŠAVIJA<sup>†</sup> AND ERIK SCHLANGEN<sup>††</sup>

<sup>\*</sup> Delft University of technology, The Netherlands  
Delft, The Netherlands  
e-mail: y.xu-5@tudelft.nl

<sup>†</sup> Delft University of technology, The Netherlands  
Delft, The Netherlands  
e-mail: B.Savija@tudelft.nl

<sup>††</sup> Delft University of technology, The Netherlands  
Delft, The Netherlands  
e-mail: Erik.Schlangen@tudelft.nl

**Key words:** Negative Poisson's ratio, Cementitious composites, cellular material, 3D printing

**Abstract:** Traditionally, mechanical properties of cementitious materials are designed “chemically”, namely by configuring their mix proportions. Owning to the development of 3D printing technology, “physical” tailoring the meso-structure of cementitious materials to design their mechanical properties becomes possible. In the present study, cementitious materials were designed both by configuring the meso-structure and the base material mix proportions. Circle and ellipse cellular structure were designed and molds for casting were prepared by 3D printing technique. Plain mortar (REF) and polyvinyl alcohol (PVA) fiber reinforced mortar (FRM) were used as base material. After casting, curing and demolding, uniaxial compression tests were performed on these cementitious cellular composites. The cellular composites exhibit three stages of compressive fracture behavior, including fracture and deformation of the cellular structure, crushing of the base material and compacting of crushed materials. With ellipse cellular design, negative Poisson's ratio was achieved during the compression and the overall energy absorption efficiency and deformability was higher than circular design cellular which implies that this cementitious cellular material be a promising impact resistant material.

### 1 INTRODUCTION

Cementitious materials are the most used construction materials in the world for their excellent properties and relatively low cost. As multi-phase materials, their mechanical properties are crucially influenced by not only the mechanical properties of their constituent phases but also the geometrical distribution of these constituents. This is normally referred to as the “micro-structure” or the “meso-structure”. Therefore, depending on the scale, the mechanical behavior of cementitious

materials can be regarded as not only the material behavior but also as structural behavior of the multi-phase system. In the past several decades, numerous efforts have been done to configure, modify or tailor the micro-structure for better performances of cementitious materials, for instance, optimize the packing density [1-3], modifying pore structure [4-6], modifying air void structure[7, 8] and introduce new phases as reinforcement of the cementitious material [9-11]. In most of these studies, admixtures or additives to configure the mix proportion are used.

Recently, as the rapid development of digital fabrication technique, materials with tailored geometrical meso-structure have attracted much attention. On one hand, the tailored geometries can give the material excellent mechanical properties such as high fracture toughness [12], high relative strength [13-15] and negative Poisson's ratio [16, 17]. On the other hand, tailoring the meso-structure also enables one more dimension of freedom of materials design: not only design the base material property but also the structural property. For cementitious materials, taking advantage the ability of 3D printing technique to fabricate complex geometries to produce cementitious cellular materials with tailored meso-structure might also be promising. Together with proper base material mix proportion, unprecedented mechanical properties of cementitious materials could be achieved.

In this work, meso-structures which possibly enable the material to have negative Poisson's ratio were designed using cementitious materials. Molds for casting cementitious materials were digitally fabricated by 3D printing technique. Consequently, the meso-structure of cementitious materials were also geometrically tailored and cementitious cellular composites were obtained. Meanwhile, different mix proportions were used as base materials. Ductility of the base material was determined by four-point bending tests and the compression behavior of cementitious cellular composites was tested under uniaxial compression. The influence of base material ductility and meso-structural design parameters on the compression behavior of cementitious cellular composites is analyzed.

## 2 MATERIALS AND METHODS

### 2.1 Materials

The matrix material was a fine-grained cementitious mortar containing CEM I 42.5 N and fly ash (FA) as binder materials. Tap water (W) was used as mixing water. Polyvinyl Alcohol (PVA) fibers produced by

Changzhou TianYi Engineering Fiber Co. Ltd was used as reinforcement by 2% in volume, physical and mechanical properties of the PVA fiber are listed in Table 1. Methylcellulose produced by Shanghai Ying Jia Industrial Development Co., Ltd. was used as viscosity modifying agent (VA) to optimize fiber distribution. Glenium 51 was used as superplasticizer to adjust mixture fluidity. The mixture proportion is given in Table 2.

**Table 1:** Properties of PVA fiber

Diameter	Length	Strength	Modulus	Density
15µm	6mm	1.6GPa	34GPa	1.28g/cm <sup>3</sup>

**Table 2:** Mixture proportion (g/L)

Mix.	Cement	FA	Sand	W	SP	PVA	VA
REF	471	556	385	428	0.86	0	0.3
FRM	471	556	385	428	0.86	25.6	0.3

### 2.2 Sample preparation

The weighted dry materials were dry-mixed for 4 minutes first, then water and superplasticizer were added into the dry mixture and mixed another 4 minutes. Hobart mixer was used as mixing machine. Afterwards, the mixture was cast into molds and covered by plastic sheet to prevent vaporization. For four-point bending specimens, Styrofoam molds were used. For uniaxial compression specimens, two different cellular structures were used: circle design (CD) and ellipse design (ED). Designing parameters of single cell of the cellular structure are shown in Figure 1. Each individual cell consists of four sections connected by four bridges. The dimensions of the specimens are shown in Figure 2. The volume of CD and ED is 67681 mm<sup>3</sup>, 75803 mm<sup>3</sup> respectively. The molds for these cellular specimens were prepared by 3D printing.

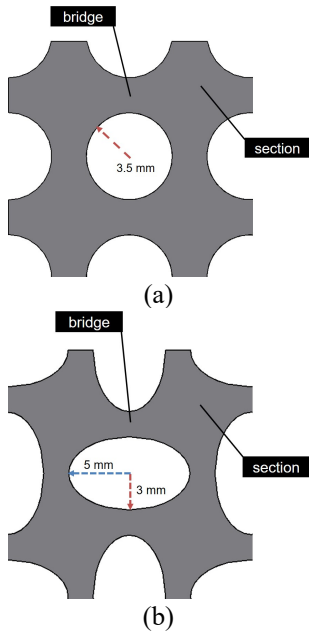


**Figure 1** Design parameters of single cell cellular structure, (a) Circle design (b) Ellipse design

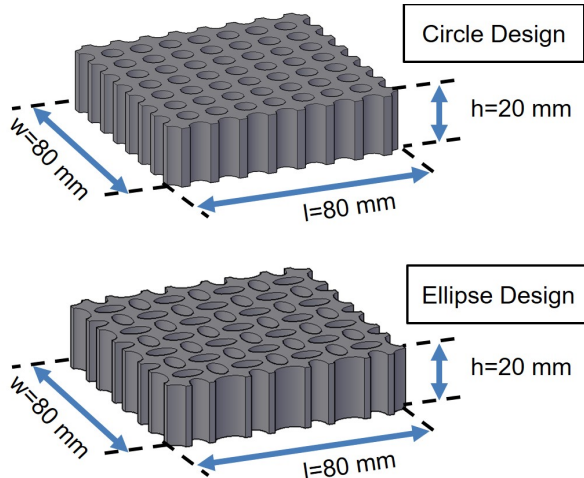


**Figure 2** Dimensions of the specimens

After one day, the cast samples were put into saturated  $\text{Ca}(\text{OH})_2$  solution and cured for 6 days and demolded before test. The specimens for four-point bending tests were cut into proper size before test. The specimens for compression test were painted with white acrylic paint and red dots were sprayed on the surface. The positions of the red dots were tracked to calculate Poisson's ratio through digital image analysis.

## 2.2 Four-point bending test

A servo hydraulic press (INSTRON 8872) was used to perform four-point bending test. A

displacement control with a constant rate of 0.005mm/s was used. The load was measured by load cell and the deflection was measured by two linear variable differential transducers (LVDTs) placed at the mid-span. Specimen size used was 180 x 30 x 8 mm. The loading set up and schematics are shown in Figure 3.

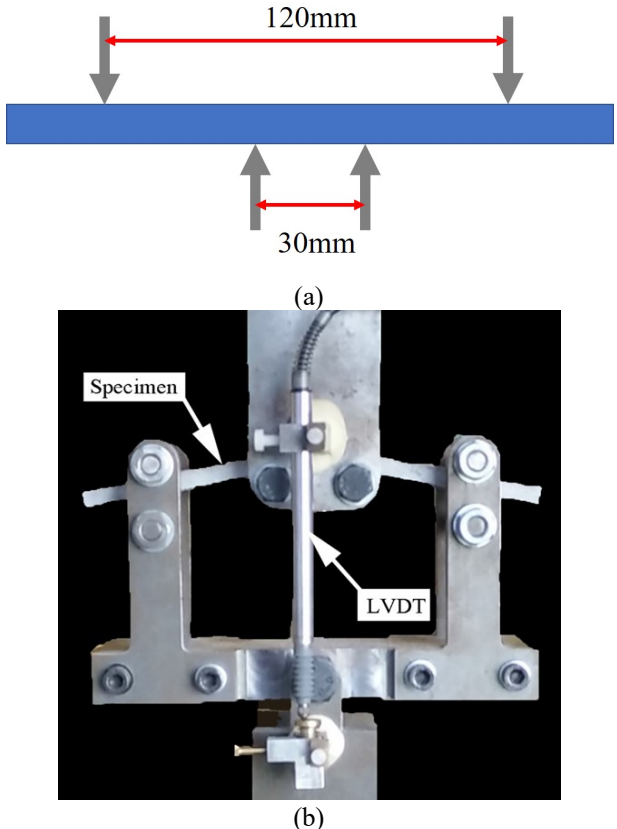


**Figure 3** (a)Schematics of four-point bending test and (b)test setup on INSTRON 8872

## 2.4 Uniaxial compressive test

The uniaxial compressive test was done by a servo hydraulic press (INSTRON 8872) under displacement control, with a constant rate of 0.01mm/s. The load and displacement are measured by the INSTRON 8872. During the test, both top and bottom surface of the specimen were covered with plastic films to reduce the friction between the specimen and loading plate.

## 3 RESULTS AND DISCUSSION

### 3.1 Base material ductility

The ductility of base material was

determined and evaluated by four-point bending tests at 7 days, three duplicates were used for each test. As can be seen from Figure 4, the REF specimens show brittle behavior under flexural load, and rather low deflection capacity can be achieved during the test. On the contrary, the FRM specimens show significantly higher ductility, even multiple cracking behavior can be observed from the flexural-deflection curve: the so-called deflection-hardening behavior was achieved during the test.

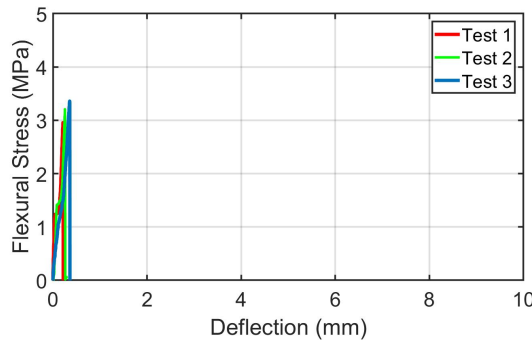


**Figure 4** Flexural Stress-deflection curve of REF specimens

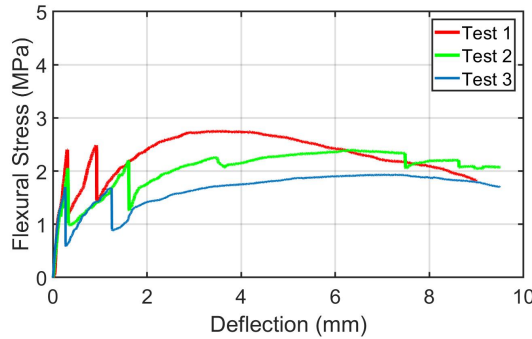
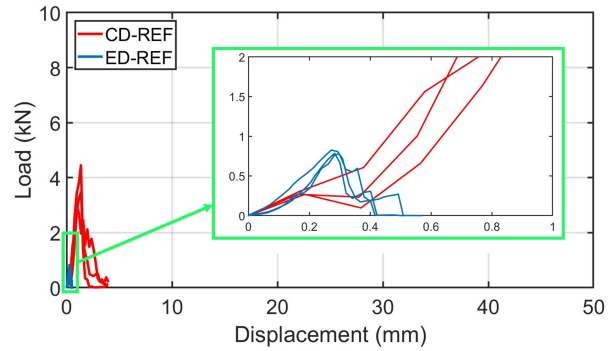


**Figure 5** Flexural Stress-Deflection curves of FRM specimens

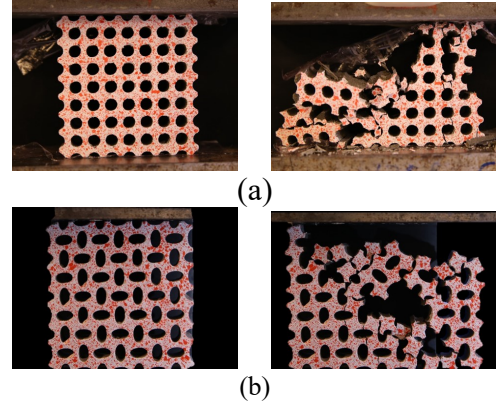
### 3.2 Response under uniaxial compression

Figure 6 shows the uniaxial compression curve of REF specimens. Both plain mortar with circle design (CD-REF) and plain mortar with ellipse design (ED-REF) show similar brittle behavior of cementitious materials under compression, namely an ascending branch can be found after loading initials, after the elastic phase, micro cracks started to appear and once peak load was reached, micro cracks localized immediately resulted in

collapse of the cellular structure and a softening branch can be observed on the load-displacement curve. Comparing to CD-REF, the ED-REF specimens have much lower peak load since the ellipse design introduced much “defects” comparing to the circle design. Because of the brittle feature of the REF mixture, only small strain can be achieved during the test which also corresponds the four-point bending test results in 3.1. Specimen before and after compression can be seen in Figure 7.



**Figure 6** Load-displacement curve of uniaxial compression test on plain mortar specimens.



**Figure 7** Specimen with (a) circle design and (b) ellipse design before and after compression

For FRM specimens, the ductility of the base material makes the compression behavior significantly different from the REF specimens (as shown in Figure 8).

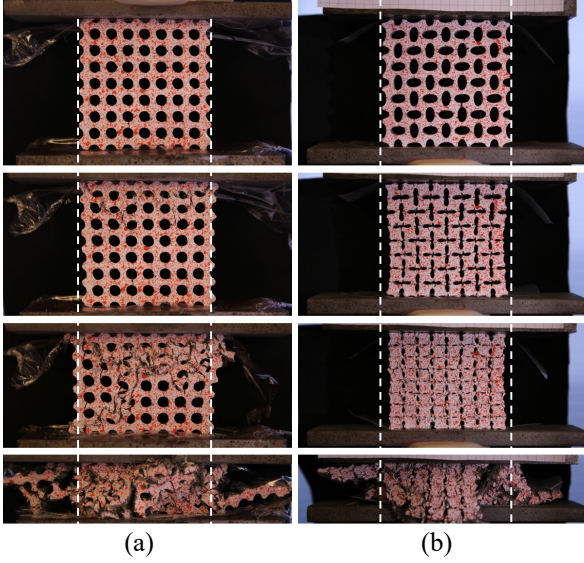


**Figure 8** Compression process of (a)CD-FRM and (b) ED FRM.

For both fiber reinforced composites with circle design (CD-FRM) and fiber reinforced composites with ellipse design (ED-REF), comparing to the brittle failure of the REF samples, three stages can be divided from the load-displacement curves.

As can be seen in Figure 9, in the first stage, similar to REF samples, one peak can be found. For CD-FRM, in the pre-peak branch multiple small cracks generated at single cells until the peak load was reached. After the peak, owing to the presence of PVA fibers, instead of rapid collapse multiple small cracks generated at single cells of the cellular structure and generally small cracks connected to be global cracks forming the typical shear plane of cementitious material under compression so that the load-displacement curve is similar to CD-REF samples in the post peak branch. For ED-FRM, as the ellipse design introduced much sharper shape at the major axis end, as a result of stress concentration small cracks mainly initiated at the bridges of each single cells in the pre-peak branch and the peak load is much lower than that of CD-FRM. While in the post-peak branch, small cracks didn't connect to be crack planes, instead, the four sections of single cells started to rotate and lateral contraction can be observed as shown in Figure 8 (b).

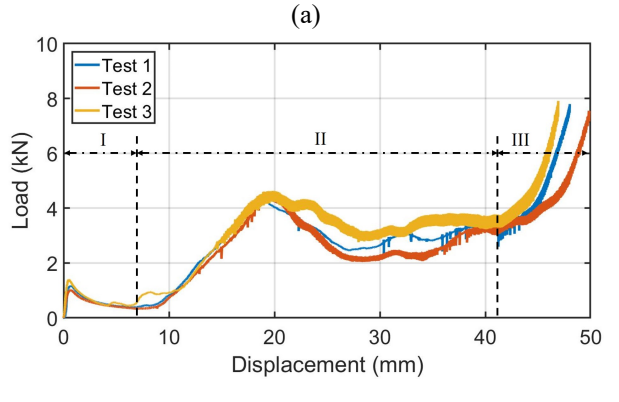
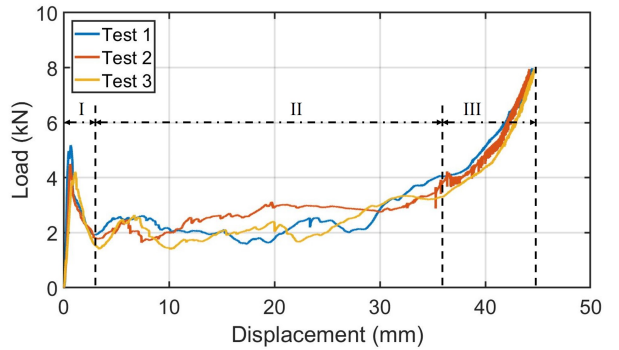


**Figure 9** Load-displacement curve of uniaxial compression test on (a) CD-FRM specimens and (b) ED-FRM specimens.

In the second stage, for CD-FRM, more small cracks generated in the sections of single cells and eventually developed to be more crack planes, leading the cellular structure to collapse layer by layer. A rather long plateau can be observed on the load-displacement curve in this stage. However, for ED-FRM, as a consequence of the rotation of the single cell sections, cracks stopped to develop from the bridge to section and the hollow ellipse structure was compressed to deform and “shrink”, exhibiting a contraction in the lateral direction when the compression continued in the vertical direction, namely negative Poisson’s ratio was achieved. Figure 10 shows the comparison of Poisson’s ratio at roughly 15mm of the compressed displacement where the ED design has the lowest Poisson’s ratio.

Because the cellular structure was compressed to be denser, the bridges connecting four sections of a single cell disappeared, resulting in the four sections starting to touch each other and bear loads. Therefore, a secondary rise can be found in the

second stage. Small cracks started to appear at the sections when the sections touched each other and then eventually the small cracks developed to be crack planes in the post peak descending branch of the secondary peak. In this sense, it is identical to the typical compression behavior of fiber reinforced cementitious material.

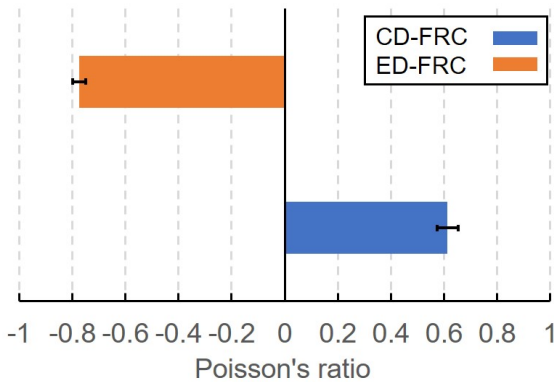


**Figure 10** Poisson's ratio of CD-FRM and ED-FRM at 15mm of uniaxial compression. Standard deviation is indicated

In the third stage, for both CD-FRM and ED-FRM, the cellular structures were entirely destroyed and it became a completely compacting process of crushed material which leads to rapid load rise because the materials were compacted denser and became stiffer. This behavior has been reported for concrete specimens under compression as well.<sup>[18]</sup>

Figure 11 shows the accumulative energy absorption of two different designs at different compressed distance. As the third stage is only a crushed material compacting process, the relative energy absorption (area below the load-displacement curve divided by the volume of each design) in this stage is not included and only calculate the value before 35mm of deformation. As the first peak load of CD-FRM is much higher than ED-FRM, in the early stage the energy absorption of CD-FRM is considerably higher. However, after the first peak, taking advantage of the negative Poisson's ratio, the energy absorption started to increase rapidly roughly at 15mm of compression which also corresponds to the displacement with the lowest Poisson's ratio. At 15mm, the meso-structure of ED-FRM is

completely compacted and the sections in each single cell started to bear load leading to a secondary rise as described before. The presence of secondary peak makes the material able to absorb more energy. Eventually the total relative energy absorption of ED-FRM is 10% higher than CD-FRM. Meanwhile, as can be seen from Figure 9, the compression tests were terminated when the load reached 8 kN in the third stage, the overall displacement of ED-FRM is also higher than CD-FRM. Considering the energy absorption and the ability of undertaking higher displacement, the CD-FRM might be a promising impact resistant material.

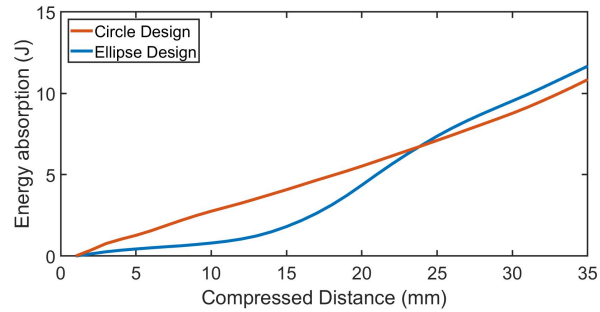


**Figure 11** Relative Energy absorption versus specimen compressed distance

## 4 CONCLUSIONS

In the present work, the compression behavior of cementitious cellular composites was studied. According to the test results, several conclusions can be drawn as follows:

- With proper meso-structural design (ellipse shape) and proper mix proportion (fiber reinforced mortar), the cementitious cellular composites exhibit negative Poisson's ratio.
- Owing to the lateral contraction, cementitious cellular composites with negative Poisson's ratio design have a higher energy absorption efficiency and higher deformation ability than the normal positive Poisson's ratio design which enables it a potential cushion material.

Directly using 3D concrete printing technique could also be possible to produce such cementitious cellular composites. Further study on this aspect will be done in the future.

## ACKNOWLEDGEMENTS

Yading Xu would like to acknowledge the funding supported by China Scholarship Council (CSC) under the grant CSC No.201708110187. The authors would like to acknowledge Mr. Jorick Wolbert for his help in sample preparation and testing.

## REFERENCES

- [1] Amario, M., Rangel, C. S., Pepe, M., & Toledo Filho, R. D. (2017). Optimization of normal and high strength recycled aggregate concrete mixtures by using packing model. *Cement and Concrete Composites*, 84, 83-92.
- [2] Li, L. G., Lin, C. J., Chen, G. M., Kwan, A. K. H., & Jiang, T. (2017). Effects of packing on compressive behaviour of recycled aggregate concrete. *Construction and Building Materials*, 157, 757-777.
- [3] Sun, Y., Wang, Z., Gao, Q., & Liu, C. (2018). A new mixture design methodology based on the Packing Density Theory for high performance concrete in bridge engineering. *Construction and Building Materials*, 182, 80-93.
- [4] Zhang, M. H., Islam, J., & Peethamparan, S. (2012). Use of nano-silica to increase early strength and reduce setting time of concretes with high volumes of slag. *Cement and Concrete Composites*, 34(5), 650-662.
- [5] Keulen, A., Yu, Q. L., Zhang, S., & Grünwald, S. (2018). Effect of admixture on the pore structure refinement and enhanced performance of alkali-activated fly ash-slag concrete. *Construction and Building Materials*, 162, 27-36.
- [6] Wang, X. F., Huang, Y. J., Wu, G. Y., Fang, C., Li, D. W., Han, N. X., & Xing, F. (2018). Effect of nano-sio 2 on strength, shrinkage and cracking sensitivity of lightweight aggregate concrete. *Construction and Building Materials*, 175, 115-125.
- [7] Qiao, M., Chen, J., Yu, C., Wu, S., Gao, N., & Ran, Q. (2017). Gemini surfactants as novel air entraining agents for concrete. *Cement and Concrete Research*, 100, 40-46.
- [8] Özcan, F., & Koç, M. E. (2018). Influence of ground pumice on compressive strength and air content of both non-air and air entrained concrete in fresh and hardened state. *Construction and Building Materials*, 187, 382-393.
- [9] Yu, J., Lin, J., Zhang, Z., & Li, V. C. (2015). Mechanical performance of ECC with high-volume fly ash after sub-elevated temperatures. *Construction and Building Materials*, 99, 82-89.
- [10] Wu, C., & Li, V. C. (2017). CFRP-ECC hybrid for strengthening of the concrete structures. *Composite Structures*, 178, 372-382.
- [11] Lu, C., Li, V. C., & Leung, C. K. (2018). Flaw characterization and correlation with cracking strength in Engineered Cementitious Composites (ECC). *Cement and Concrete Research*, 107, 64-74.
- [12] Li, T., Chen, Y., & Wang, L. (2018). Enhanced fracture toughness in architected interpenetrating phase composites by 3D printing. *Composites Science and Technology*, 167, 251-259.
- [13] Hu, Z., Thiagarajan, K., Bhushal, A., Letcher, T., Fan, Q. H., Liu, Q., & Salem, D. (2017). Design of ultra-lightweight and high-strength cellular structural composites inspired by biomimetics. *Composites Part B: Engineering*, 121, 108-121.
- [14] Maurath, J., & Willenbacher, N. (2017). 3D printing of open-porous cellular ceramics with high specific strength. *Journal of the European Ceramic Society*, 37(15), 4833-4842.
- [15] Ryvkin, M., & Shraga, R. (2018). Fracture toughness of hierarchical self-similar honeycombs. *International Journal of Solids and Structures*, 152, 151-160.
- [16] Greaves, G. N., Greer, A. L., Lakes, R. S., & Rouxel, T. (2011). Poisson's ratio and modern materials. *Nature materials*, 10(11), 823.
- [17] Han, Y., & Lu, W. (2018). Evolutionary design of nonuniform cellular structures

- with optimized Poisson's ratio distribution. *Materials & Design*, 141, 384-394.
- [18] Van Mier, J.G.M., 1997. Fracture Processes of Concrete. CRC Press.